Journal of The Electrochemical Society, **156** (6) B735-B742 (2009)
0013-4651/2009/156(6)/B735/8/$25.00 © The Electrochemical Society

Displacement Reaction in Pulse Current Deposition of PtRu for Methanol Electro-Oxidation

Yu-Chi Hsieh,* Pu-Wei Wu,,z Yung-Jean Lu, and Yun-Min Chang***

Department of Materials Science and Engineering, National Chiao Tung University, Hsin-chu 300, Taiwan

Galvanostatic depositions in rectangular pulses and nitrosol precursors were employed to prepare PtRu nanoparticles on carbon clothes in various sizes and compositions. Variables including current on-time (T_{on}), current off-time (T_{off}), and current density were explored to identify the optimized catalytic performances for methanol electro-oxidation. Electrochemical characterizations including cyclic voltammetry and hydrogen desorption were carried out. Images from a transmission electron microscope on the PtRu nanoparticles revealed a moderate size distribution. Signals from X-ray patterns indicated a slight shift of diffraction peaks, suggesting that the Ru was alloyed successfully in the Pt lattice. In addition, the amount of alloyed Ru was found to decrease with reduced duty cycles. Composition determinations from inductively coupled plasma mass spectrometry and analysis on the oxidation states from X-ray photoelectron spectroscopy suggested a displacement reaction in which the Ru was alternately deposited and dissolved during T_{on} and T_{off}, while the Pt was deposited continuously. As a result, we observed substantial enrichment of Pt in the PtRu nanoparticles when the duty cycle was shortened.
 [DOI: 10.1149/1.3116187]

Manuscript submitted November 3, 2008; revised manuscript received January 22, 2009. Published April 16, 2009.

Development of clean and affordable energy has attracted considerable attention due to rising concerns over oil price and harmful CO_2 emission. Among the possible systems under study, the direct methanol fuel cell (DMFC) is recognized as a promising power source for applications in portable electronics and transportations.[1,2] Because electro-oxidation of methanol is intrinsically slow, many materials have been investigated as electrocatalysts at the anode. They include alloys in binary, tertiary, and quaternary compositions such as PtRu, PtCo, PtRuCo, and PtRuNiZr.[3-7] So far, the PtRu has appeared as the leading candidate with superb electrocatalytic performance. It is because by alloying with Ru, the undesirable Pt poisoning by CO could be largely reduced. Mechanisms including bifunctional effect and ligand model are proposed to explain the contributory role of Ru while alloying with Pt.[8,9] Moreover, the catalytic behaviors of PtRu depend greatly on its surface composition. For example, Richarz et al. prepared the Pt_xRu_{1-x} in various compositions and determined the $Pt_{0.5}Ru_{0.5}$ to possess the highest activity for methanol electro-oxidation.[10]

In practice, the PtRu is impregnated on appropriate carbon supports for an extended reaction interface. Conventional synthetic approaches for the PtRu-catalyzed electrodes entail techniques in chemical reduction and hydrogen annealing.[11,12] These methods add substantial difficulties in controlling the locations and compositions of the resulting PtRu nanoparticles. In contrast, approaches involving electrochemical reductions are rather straightforward. Because the growths of PtRu nanoparticles are occurring selectively at the interface between electrode and electrolyte, the electrodeposition routes are recognized to produce electrodes with exceptional efficiencies in the catalyst utilization, albeit with moderate size distributions.[13,14] Because the nuclei formation and growth are extremely sensitive to the overpotentials imposed, potentiostatic and galvanostatic depositions are known to produce distinct morphologies and compositions in the resulting PtRu nanoparticles. Between them, the galvanostatic deposition is suitable to prepare catalysts in a larger geometric area and better distributions, in addition to simpler operation setups.[15-18]

In the galvanostatic depositions, the driving forces are imposed in manners of direct current or pulse current (pc). With a single variable in current density (J_a), the dc deposition is known to produce dendritic morphologies, because growths of the deposit are capped by the mass transport at a diffusion-limiting current.[19] In contrast, deposition in the pc mode allows independent adjustments of J_a, current on-time (T_{on}), and current off-time (T_{off}), offering more opportunities to obtain deposits with desirable attributes. As a result, many groups have employed pc depositions to fabricate electrocatalysts in Pt and PtRu.[15-17,20-22] For example, Choi et al. reported notable advantages of pc deposition in particle sizes, adhesions, and uniform distributions.[22]

During the T_{off} in a pc deposition for binary alloys, differences in the redox potentials for the deposited metals often render a spontaneous galvanostatic displacement reaction in which the constituent of less positive redox potential dissolves from the deposit while the one with a higher redox potential is reduced from the electrolyte. A well-studied system is the CuNi alloy where detailed theoretic modeling and experimental results were discussed.[23-25] In this system, the Ni was alternately deposited and dissolved during T_{on} and T_{off}, while the Cu was deposited continuously. Hence, the ratio for the T_{on}/T_{off} played an important role in determining the resulting CuNi composition. So far, many groups have employed the displacement reaction to prepare substrates with unique surface layers.[26-30] For instance, noble films of Au, Pd, and Pt were deposited on Ge substrates with reasonable adhesions.[30] In addition, Brankovic et al. have explored the spontaneous depositions of Pt on both single-crystalline and nanoparticulate Ru surfaces.[31-33] In Ru single crystals, they believe the surface oxidations are responsible for the reduction of $PtCl_6^{2-}$ from the electrolyte. However, in the case of nanoparticles, partial dissolutions of Ru are likely to contribute to the $PtCl_6^{2-}$ reductions.

To date, many groups have employed pc deposition to fabricate PtRu nanoparticle and characterize their electrochemical performances.[15,16,19-21] However, none of them discussed the possible influences of displacement reaction in determining the resulting PtRu compositions. In this work, we investigate relevant variables to identify the effect of displacement reaction by carrying out careful analysis on the compositions and associated methanol electro-oxidation behaviors.

Experimental

A carbon cloth (E-TEK) was used as the starting substrate for the growth of PtRu. Prior to the pc deposition process, the carbon cloth was coated with an ink dispersion in which 5.0 mg Nafion solution (5.0 wt %) and 8.0 mg carbon powders (Vulcan XC-72R) were mixed in 5.0 mL of 99.5 wt % ethanol for 30 min. The ink dispersion was deposited repeatedly on a 2×2 cm^2 carbon cloth which was kept at 80°C atop a hot plate to evaporate the residual solvent. The weight of the coated electrode was 26.3 mg/cm^2. Subsequently, an electrochemical conditioning step was conducted by imposing five voltammetric scans on the coated carbon cloth at potentials between −0.2 and +1.1 V (vs Ag/AgCl) at a scan rate of 50 mV/s in

* Electrochemical Society Student Member.
** Electrochemical Society Active Member.
z E-mail: ppwu@mail.nctu.edu.tw

an electrolyte of 0.5 M H_2SO_4. The purpose for this treatment was to homogenize the coated carbon cloth and expose a larger effective surface area.

The plating bath for the electrodeposition was formulated by mixing 99.9 wt % $RuCl_3$ (Sigma-Aldrich) and 97.0 wt % $NaNO_2$ (Showa) in an aqueous solution at 100°C for 1.0 h, followed by dissolution of 99.9 wt % H_2PtCl_6. Afterward, the solution was cooled to room temperature, with the addition of 97.0 wt % H_2SO_4 (Showa) to increase conductivity of the electrolyte. The resulting concentrations for the H_2PtCl_6, $RuCl_3$, $NaNO_2$, and H_2SO_4 were 0.005, 0.005, 0.050, and 0.250 M, respectively. The solution was aged for 2 weeks to reach a steady state for the complex ions. In the pc depositions, rectangular pulses with independent parameters in T_{on}, T_{off}, and J_a were explored. Three sets of experiments were designed to elucidate the effect of displacement reaction. First, T_{on} of 50 ms and J_a of 50 mA/cm^2 were selected with the T_{off} varied between 100 and 600 ms. Second, T_{off} of 400 ms and J_a of 50 mA/cm^2 were chosen with the T_{on} varied between 25 and 400 ms. Lastly, we maintained the T_{on} and T_{off} at 50 and 400 ms but adjusted the J_a between 75 and 200 mA/cm^2. Throughout our experiments, the total coulombic charge was kept at 8.0 C/cm^2. Once the deposition was completed, the carbon cloth was removed and washed for subsequent electrochemical characterizations.

The electrochemical measurements were conducted at 26°C in a three-electrode arrangement using an EG&G 263A. First, to evaluate the electrochemical surface area (ECSA), the PtRu-catalyzed carbon clothes were subjected to cyclic voltammetric (CV) scans in the voltage range of −0.2 and 0.9 V in 0.5 M H_2SO_4 with a scan rate of 50 mV/s. The ECSA was estimated by the integrated charge in the hydrogen desorption region.[34,35] Next, for catalytic abilities on the methanol electro-oxidation, multiple CV sweeps were performed in a potential range of −0.2 and 0.9 V at a scan rate of 20 mV/s in 500 mL of 0.5 M H_2SO_4 and 1.0 M CH_3OH. The area for the working electrode was 1.0 cm^2. The Ag/AgCl and Pt foil (10.0 cm^2) were used as the reference and counter electrodes, respectively. The CV scan at the second cycle was used for comparison purposes.

For phase confirmation of the deposited PtRu nanoparticles, X-ray diffraction (XRD, Siemens D5000) with a K_α of 1.54 Å was employed. A transmission electron microscope (TEM, Philips Tecnai-20) was used to observe the morphologies and distributions for the PtRu nanoparticles. The average sizes and standard deviations of the PtRu nanoparticles were obtained by analyzing images from the TEM through software (Image-Pro Plus 6.0). Catalyst loadings of the PtRu after the pc depositions were determined by an inductively coupled plasma mass spectrometry (ICP-MS, SCIEX ELAN 5000), where the samples were dissolved in a solution containing HCl, HNO_3, and HF at 2:2:1 volume ratio. X-ray photoelectron spectroscopy (XPS, Thermo Microlab 350) was used to confirm the oxidative states of Ru in the PtRu nanoparticles.

Results and Discussion

Previously, several reports have identified the nitroso compounds of Ru to be promising complexes as the Ru sources for PtRu electrodepositions.[36-38] When dissolved in an acidic electrolyte, a spontaneous Ru deposition was not observed in nitroso precursors as compared to the typical $RuCl_3$.[39] This contributed to a longer lifetime and minimal bath management. In addition, Gavrilov et al. indicated that the presence of nitroso ligands shifts Ru/Ru(III) redox potential to more positive values.[40] Therefore, with the selection of nitroso precursor, similar Pt:Ru ratios are expected to be obtained in both deposit and solution states. This is especially critical because previous studies using the $RuCl_3$ and $RuCl_5$ reported substantial Pt enrichments with respect to their concentration ratios in the electrolyte. Consequently, their fabrications of desirable PtRu compositions hinged on empirical determination entirely.

Our preparation steps of nitroso Ru precursor followed earlier documentation in which the dissolution of $RuCl_3$ in excess $NaNO_2$ at elevated temperatures was carried out.[41] The resulting complex was confirmed by Blake et al. to be $Ru(NO)(NO_2)_4(OH)^{2-}$.[42] However, in our electrolyte we also added H_2PtCl_6 after the formation of Ru nitroso complex. Because the molar ratio for Pt:Ru:$NaNO_2$ was 1:1:10, we surmise that the simultaneous presence of $PtCl_6^{2-}$ and $Pt(NO_2)_xCl_{6-x}^{2-}$ is likely. The color for the plating bath is in light yellow. This is in sharp contrast with the electrolytes of $RuCl_3$ and $RuCl_5$, which appear in dark brown.

For the pc depositions, intricate interactions between T_{on}, T_{off}, and J_a exert significant influences over the PtRu catalyst loadings, compositions, distributions, as well as particle sizes. Therefore, careful scrutiny in the plating variables would be necessary. In our first set of experiments, pc depositions were conducted at various T_{off}, while the T_{on} and J_a remained unchanged at 50 ms and 50 mA/cm^2, respectively. Because we maintained the total charge constant at 8.0 C/cm^2, the entire deposition process lasted approximately 4–35 min. Table I lists the experimental parameters as well as results from TEM and ICP-MS for the PtRu nanoparticles. As presented, the PtRu loadings were in the range of 67.6–128.5 μg/cm^2. Following faradaic law, the coulombic efficiencies were estimated at 1.8–3.6%. These reduced values are attributed to the parasitic hydrogen evolution occurring on the Pt surfaces. Currents from the capacitive charge and discharge were not expected to be substantial, as the effective working range for the capacitance component were less than 1.0 ms for T_{on} and T_{off}.[20] We observed a notable trend for the PtRu composition on different pulses. The ratio for the Pt in the PtRu nanoparticles increased considerably with a longer T_{off}. At the shortest T_{off} of 100 ms, we determined the composition to be $Pt_{52.7}Ru_{47.3}$. In contrast, at the largest T_{off} of 600 ms, the makeup was confirmed as $Pt_{83.4}Ru_{16.6}$.

TEM observations on the particles sizes indicated a slightly wider distribution as compared to those from conventional chemical reduction methods. For example, at a T_{off} of 200 ms, the PtRu nanoparticles were an average of 12.9 nm with a standard deviation of 8.7 nm. Moderate size distributions are typical, because the nucleation and growth took place during each individual pulse. A recent report by Bennett et al. also observed similar behaviors when they prepared Pt nanoparticles on diamond thin films.[43] Figure 1 provides the representative TEM images for the PtRu nanoparticles from T_{off}

Table I. Results from material characterizations on the PtRu nanoparticles with fixed values of T_{on} (50 ms), J_a (50 mA/cm^2), and total coulombic charge (8.0 C/cm^2).

T_{off} (ms)	Pt loading (μg/cm^2)	Ru loading (μg/cm^2)	Pt/Ru atomic ratio	Total loading (μg/cm^2)	Average size (nm)	Standard deviation
100	62.5	28.9	52.8/47.2	91.4	7.2	5.6
200	89.8	38.7	54.6/45.4	128.5	12.9	8.7
300	64.0	21.0	61.2/38.8	85.0	6.6	5.4
400	52.4	15.2	64.1/35.9	67.6	4.1	2.8
500	78.5	11.5	77.9/22.1	90.0	6.3	4.7
600	100.8	10.4	83.4/16.6	111.2	11.3	9.4

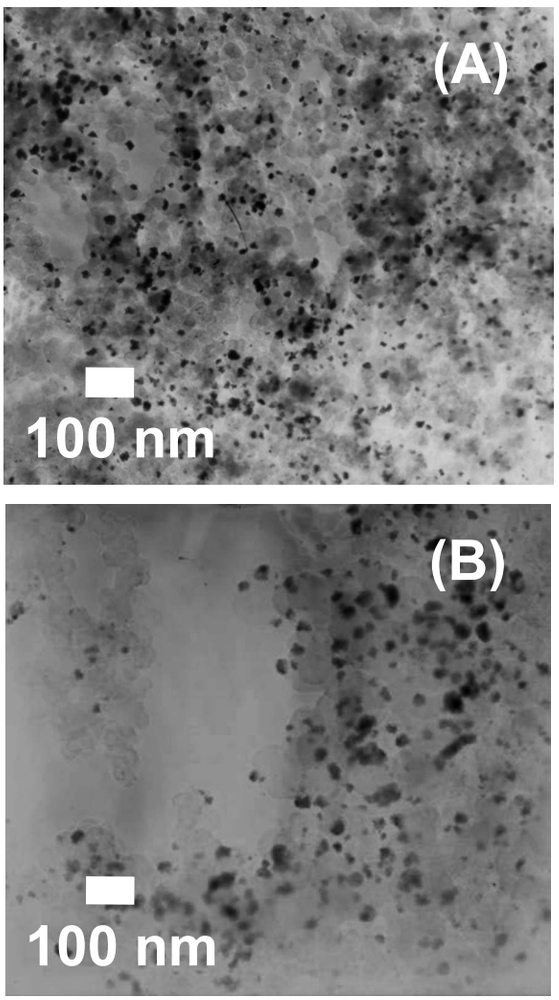

Figure 1. Representative TEM images for the PtRu nanoparticles with fixed values of T_{on} (50 ms), J_a (50 mA/cm^2), and coulombic charge (8.0 C/cm^2), as well as T_{off} of (A) 400 and (B) 600 ms.

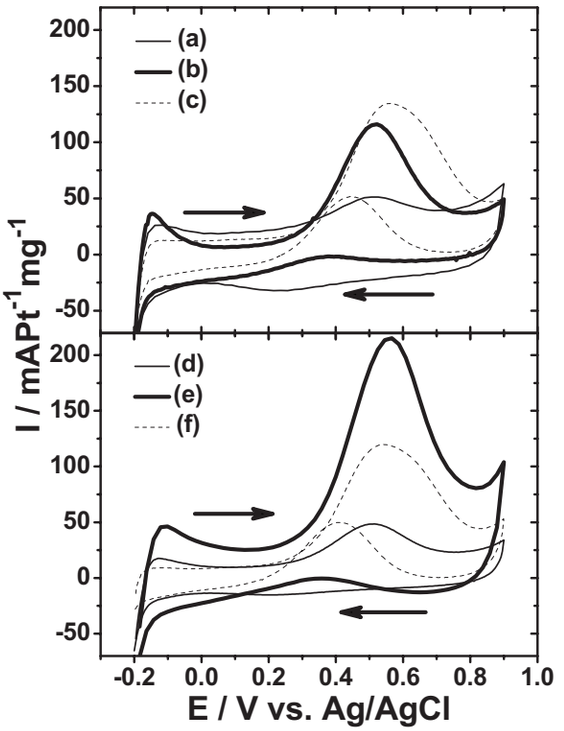

Figure 2. CV profiles in mass activity for the PtRu-catalyzed carbon clothes with fixed values of T_{on} (50 ms), J_a (50 mA/cm^2), and coulombic charge (8.0 C/cm^2), as well as T_{off} of (a) 100, (b) 300, (c) 500, (d) 200, (e) 400, and (f) 600 ms.

of 400 and 600 ms, respectively. The average size of the PtRu nanoparticles from the T_{off} of 400 ms was 4.1 nm, while the T_{off} of 600 ms revealed a somewhat larger size of 11.3 nm. These TEM images also indicated that the PtRu nanoparticles were dispersed uniformly on the carbon substrates with negligible aggregation.

Figure 2 exhibits the CV profiles in mass activity for the PtRu-catalyzed electrodes at various T_{off}. Critical information from the CV responses, including the onset potentials, peak current (i_a) and potential (V_a) at anodic scans, peak current (i_c) and potential (V_c) at cathodic scans, as well as values for ECSA, are listed in Table II. For the samples with T_{off} in 100 and 200 ms, their CV curves revealed moderate current outputs. This is unexpected, because compositions for these two samples were $Pt_{52.8}Ru_{47.2}$ and $Pt_{54.6}Ru_{45.4}$, respectively. In contrast, the CV profiles of the remaining samples demonstrated obvious anodic signals with relatively reduced ca-

Table II. Electrochemical parameters from the CV scans in mass activity of the PtRu-catalyzed carbon clothes with fixed values of T_{on} (50 ms), J_a (50 mA/cm^2), and total coulombic charge (8.0 C/cm^2).

	Anodic scan		Cathodic scan			
T_{off} (ms)	V_a[a] (mV)	i_a[b] mA/(Pt mg)	V_c[c] (mV)	I_c[d] mA/(Pt mg)	ECSA[e] (cm^2/Pt mg)	i_a/i_c
100	516.3	52.5	NA	NA	251.0	NA
200	509.8	48.9	NA	NA	209.3	NA
300	521.2	116.5	387.5	NA	477.3	NA
400	560.4	213.8	360.0	0.7	751.4	304
500	558.7	133.4	448.6	51.1	286.0	2.61
600	541.6	119.8	407.0	50.1	152.5	2.39

[a] Potential at peak mass activity in anodic scan.
[b] Peak mass activity in anodic scan.
[c] Potential at peak mass activity in cathodic scan.
[d] Peak mass activity in cathodic scan.
[e] ECSA from hydrogen desorption data.

Table III. Results from material characterizations on the PtRu nanoparticles with fixed values of T_{off} (400 ms), J_a (50 mA/cm^2), and total coulombic charge (8.0 C/cm^2).

T_{on} (ms)	Pt loading (μg/cm^2)	Ru loading (μg/cm^2)	Pt/Ru atomic ratio	Total loading (μg/cm^2)	Average size (nm)	Standard deviation
25	92.3	4.7	90.9/9.1	97.0	6.7	5.0
50	52.4	15.2	64.1/35.9	67.6	4.1	2.8
100	88.8	40.0	53.7/46.3	128.8	8.3	5.2
200	56.1	27.3	51.5/48.5	83.4	8.7	5.0
400	48.1	22.5	52.5/47.5	70.6	8.4	7.4

thodic signals, suggesting considerable abilities for the methanol electro-oxidation. In addition, the onset potentials became smaller when the amount of Ru was increased, a fact that is consistent with what was reported in literature that alloying with Pt promotes methanol electro-oxidation.[4] The ratio for the i_a/i_c indicates the capabilities to remove CO after methanol dehydrogenation. Among these samples, the one with T_{off} of 400 ms demonstrated the highest value. As expected, for the mass activities, the sample with T_{off} in 400 ms exhibited the highest value of 213 mA mg^{-1} Pt^{-1}. Moreover, the general trend for the ECSA was consistent with that of i_a, in which a larger ECSA is associated with a higher i_a.

In our second set of experiments, the pc depositions were carried out at various T_{on} while the T_{off} and J_a were held at 400 ms and 50 mA/cm^2, respectively. Because we kept the total charge unchanged at 8.0 C/cm^2, the entire deposition process lasted approximately 2.6–45.0 min. Table III provides the experimental conditions as well as results from TEM and ICP-MS for the PtRu nanoparticles. As listed, the PtRu loadings were in the range of 67.6–128.8 μg/cm^2. Similarly, the coulombic efficiency was estimated at 1.8–2.6%. These values were in line with results obtained from our first set of experiments. An interesting trend was observed in which a longer T_{on} resulted in a lower amount of Pt in the PtRu nanoparticles. At the shortest T_{on} of 25 ms, we recorded the composition to be $Pt_{90.9}Ru_{9.1}$. In contrast, at the largest T_{on} of 400 ms, a composition of $Pt_{52.5}Ru_{47.5}$ was measured.

TEM observations on the PtRu nanoparticles confirmed a similar pattern in the size distributions. For example, at a T_{on} of 25 ms, we obtained the average size to be 6.7 nm with a standard deviation of 5.0 nm. At a larger T_{on} of 400 ms, the average size was 8.4 nm with a standard deviation of 7.4 nm. Representative TEM pictures from those two samples are provided in Fig. 3. Consistent with images in Fig. 1, the PtRu nanoparticles were deposited uniformly throughout the substrates without aggregation. Figure 4 demonstrates the CV profiles in mass activity for the PtRu nanoparticles at various T_{on}. Relevant parameters from the CV responses are also provided in Table IV. Apparently, all the samples revealed obvious anodic peaks without notable cathodic peaks. They suggest the presence of reasonable catalytic behaviors for methanol electro-oxidation. As expected, the onset potentials and the peak potentials at the anodic scans became smaller with increasing Ru amounts. The sample with a T_{on} of 50 ms revealed the highest mass activities, reaching values at 213.8 mA mg^{-1} Pt^{-1}. Similarly, the trend of ECSA agreed with that of i_a, a fact we established in the previous set of experiments.

We realized that the duty cycle, defined as $T_{on}/(T_{on} + T_{off})$, would be an appropriate indicator to solicit further information on the composition variations over T_{on} and T_{off}. As defined, a higher duty cycle is closer to the dc deposition, while a lower one represents a longer stop time between pulses. Figure 5 exhibits the ratio of Pt in the PtRu nanoparticles as a function of duty cycle from the data listed in Tables I and III. Remarkably, the Pt ratio increased rapidly as the duty cycle was reduced. This infers that a longer T_{off} renders a pronounced effect of Ru loss in the PtRu nanoparticles. At higher duty cycles, we reached a plateau, with the resulting composition approaching $Pt_{52}Ru_{48}$. These behaviors were expected, because the galvanostatic deposition from nitroso precursors of Pt and Ru were likely to reproduce their concentration ratios in the electrolyte on the PtRu nanoparticles. In order to verify the observed trend, we also performed the pc depositions with J_a of 75, 100, and 200 mA/cm^2, leaving the T_{on} and T_{off} fixed at 50 and 400 ms, respectively. The experimental parameters and resulting material characteristics are provided in Table V. Interestingly, the Pt amounts

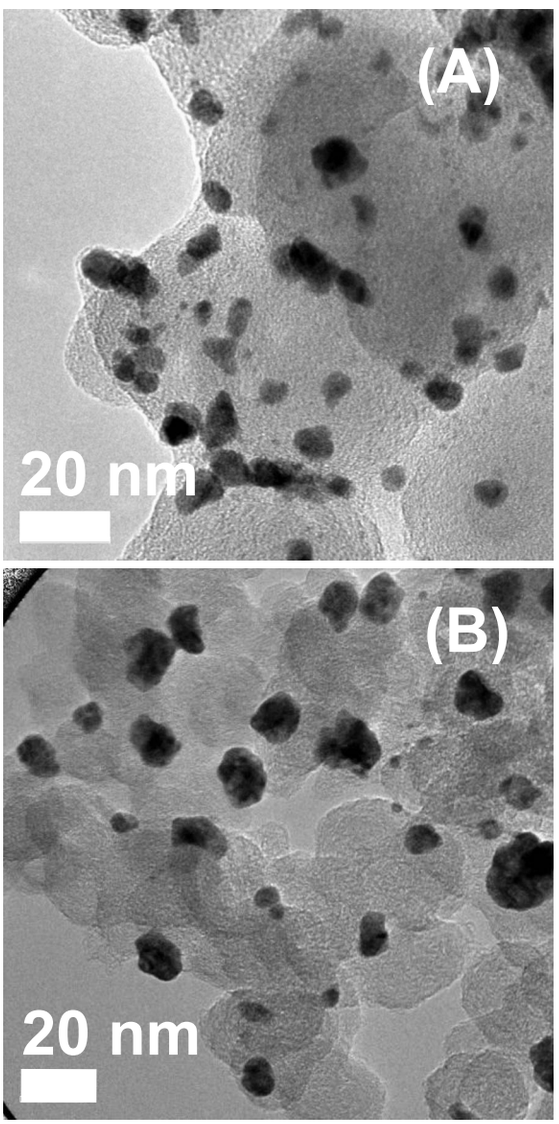

Figure 3. Representative TEM images for the PtRu nanoparticles with fixed values of T_{off} (400 ms), J_a (50 mA/cm^2), and coulombic charge (8.0 C/cm^2), as well as T_{on} of (A) 25 and (B) 400 ms.

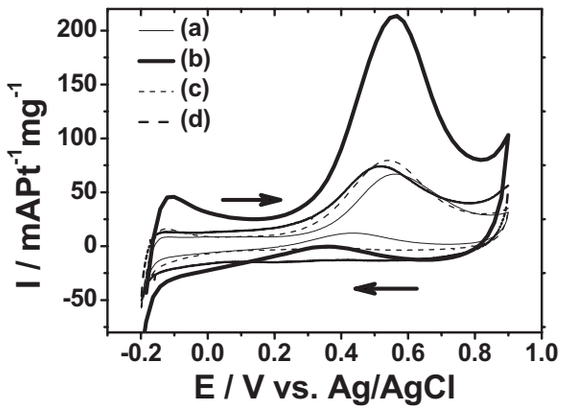

Figure 4. CV profiles in mass activity for the PtRu-catalyzed carbon clothes with fixed values of T_{off} (400 ms), J_a (50 mA/cm^2), and coulombic charge (8.0 C/cm^2), as well as T_{on} of (a) 25, (b) 50, (c) 100, and (d) 400 ms.

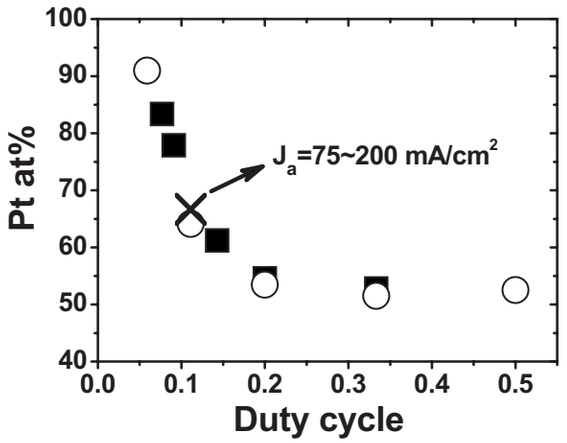

Figure 5. The effect of duty cycle on the Pt atomic ratio for the PtRu nanoparticles. Data are from Tables I (■), III (○), and V (×).

from these samples were rather consistent, indicating that the pc deposition was insensitive to the current densities under study once the T_{on} and T_{off} were determined. In addition, the catalyst loadings were in the range of 49.1–67.6 μg/cm^2, values that are in line with earlier results. Table VI also lists the electrochemical characteristics for these samples.

To account for the apparent enrichment in the Pt at shorter duty cycles, we believe a displacement reaction was taking place where the Ru in the PtRu nanoparticles was preferentially dissolved while the Pt cations in the solution were reduced during T_{off}. This is attributed to the observed rise in the Pt ratio when the T_{off} was prolonged. The nature of displacement reaction could be supported by detailed XRD analysis on the PtRu nanoparticles to determine their lattice parameter. Figure 6 exhibits the XRD patterns for the PtRu nanoparticles with T_{off} of 100, 400, and 600 ms, respectively. The complete parameters for their synthetic conditions are shown in Table I. Due to the interferences from carbon clothes, the XRD profiles were expectedly rough. Nevertheless, the signals from Pt(111), Pt(200), Pt(220), and carbon were identified. Because we did not observe the characteristic Ru peaks, we rationalize that alloying of Ru into the Pt lattice was successfully achieved. Moreover, because the atomic radius of Ru is smaller than that of Pt, substitution of Ru in the Pt unit cell results in the reduction of lattice parameters. This engenders a slight shift of diffraction peaks to larger angles. To minimize undesirable noises, we selected the signal from Pt(111), as shown in Fig. 7, to estimate the lattice parameter with the equation below

$$a = \frac{\sqrt{3}\lambda_{k\alpha}}{2 \sin \theta_{max}} \quad [1]$$

Where a is the lattice parameter, θ_{max} is the peak position for Pt(111), and $\lambda_{k\alpha}$ is the wavelength of X-ray. The value for a could

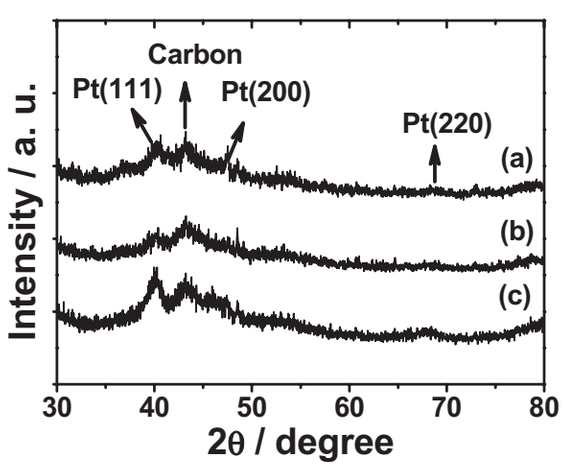

Figure 6. The XRD patterns for the PtRu nanoparticles with fixed values of T_{on} (50 ms), J_a (50 mA/cm^2), and coulombic charge (8.0 C/cm^2), as well as T_{off} of (a) 100, (b) 400, and (c) 600 ms.

Table IV. Electrochemical parameters from the CV scans in mass activity of the PtRu-catalyzed carbon clothes with fixed values of T_{off} (400 ms), J_a (50 mA/cm^2), and total coulombic charge (8.0 C/cm^2).

	Anodic scan		Cathodic scan			
T_{on} (ms)	V_a (mV)	i_a[b] mA/(Pt mg)	V_c (mV)	I_c mA/(Pt mg)	ECSA[e] (cm^2/Pt mg)	i_a/i_c
25	565.1	66.3	433.1	12.7	105.0	5.20
50	560.4	213.8	360.0	0.7	751.4	304
100	540.0	81.2	NA	NA	188.9	NA
200	539.2	100.1	NA	NA	296.0	NA
400	518.0	108.7	NA	NA	130.4	NA

[a] Potential at peak mass activity in anodic scan.
[b] Peak mass activity in anodic scan.
[c] Potential at peak mass activity in cathodic scan.
[d] Peak mass activity in cathodic scan.
[e] ECSA from hydrogen desorption data.

Table V. Results from material characterizations on the PtRu nanoparticles with fixed values of T_{on} (50 ms), T_{off} (400 ms), and total coulombic charge (8.0 C/cm^2).

J_a (mA/cm^2)	Pt loading (μg/cm^2)	Ru loading (μg/cm^2)	Pt/Ru atomic ratio	Total loading (μg/cm^2)	Average size (nm)	Standard deviation
75	39.1	10.0	66.8/33.2	49.1	7.2	5.9
100	42.4	10.9	66.7/33.3	53.3	11.4	8.9
200	49.9	13.0	66.5/33.5	62.9	14.3	9.6

Table VI. Electrochemical parameters from the CV scans in mass activity of the PtRu-catalyzed carbon clothes with fixed values of T_{on} (50 ms), T_{off} (400 ms), and total coulombic charge (8.0 C/cm^2).

	Anodic scan		Cathodic scan			
J_a (mA/cm^2)	V_a[a] (mV)	i_a[b] mA/(Pt mg)	V_c[c] (mV)	I_c[d] mA/(Pt mg)	ECSA[e] (cm^2/Pt mg)	i_a/i_c
75	531.8	197.7	386.0	3.8	526.8	51.2
100	524.5	138.9	Na	NA	434.5	NA
200	487.0	37.4	Na	NA	243.4	NA

[a] Potential at peak mass activity in anodic scan.
[b] Peak mass activity in anodic scan.
[c] Potential at peak mass activity in cathodic scan.
[d] Peak mass activity in cathodic scan.
[e] ECSA from hydrogen desorption data.

further be used to deduce the amount of alloyed Ru, as suggested by Antolini et al., in the following relation[44]

$$a = a_0 - 0.124x_{Ru} \quad [2]$$

where a_0 is the standard lattice parameter from a bulk Pt (JCPDS: 870646) and x_{Ru} is the atomic Ru ratio in the alloyed state. The results from these estimations are presented in Table VII. As listed, we noticed that when the T_{off} was prolonged, the ratio for the alloyed Ru also decreased. This behavior is understandable, because when the displacement reaction was occurring (at larger T_{off}), the Ru on the surface were dissolved preferentially, leaving those buried inside (the alloyed Ru) intact.

An alternative explanation for the Pt enrichment at shorter duty cycles is a cementation process. As proposed by Spendelow and Wieckowski, spontaneous deposition of Pt from electrolyte could proceed via the oxidation of Ru substrate.[45] In such a reaction, the Ru is not dissolved but exists in an oxidized state on the surface with metallic Pt deposited from the electrolyte. This model poses a drastic contrast with that of displacement reaction, where the Ru is dissolved. Therefore, we could identify the exact mechanism in our case simply by determining the oxidative states of Ru at different duty cycles.

Figure 8a presents the XPS signals from Ru ($3p_{3/2}$) on samples of T_{off} in 100, 400, and 600 ms, respectively. The complete synthetic parameters can be obtained in Table I. The selection of Ru ($3p_{3/2}$) instead of Ru ($3d_{5/2}$) was to avoid possible interference from that of C (1 s). As shown in the diagram, all the samples revealed rather broad profiles. The signals peaks were located at 462.2, 462.0, and 461.9 eV for samples of 100, 400, and 600 ms, respectively. Earlier, the peak for metallic Ru was documented at 461.1 eV, which was close to what we measured.[46] A slight deviation is expected, because there is a minor shift of Ru signals (less than 0.1 eV) in the PtRu from that of metallic Ru.[47] Nevertheless, our broad signals seem to suggest that Ru existed in multiple oxidative states. Furthermore, the XPS signal intensity decreased considerably with longer T_{off}, indi-

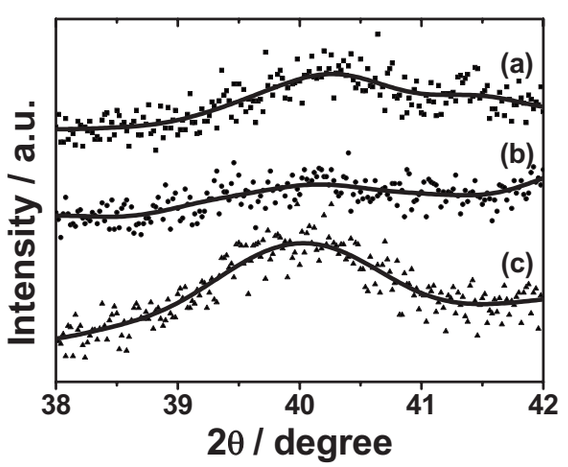

Figure 7. XRD patterns from Fig. 6 with an enlarged range between 38 and 42° for lattice parameter determination.

Table VII. Lattice parameter and alloyed Ru for the PtRu nanoparticles with fixed values of T_{on} (50 ms), J_a (50 mA/cm^2), and coulombic charge (8.0 C/cm^2).

Sample	Pt (111) (deg)	Lattice parameter a (Å)	X_{Ru} (%)	Pt/Ru ratio[b]
TF100	40.21	3.879	33.9	52.8/47.2
TF400	40.16	3.884	30.2	64.1/35.9
TF600	39.97	3.902	15.9	83.4/16.6
Pt[a]	39.79	3.920		

[a] From JCPDS 870646.
[b] From ICP-MS (as shown in Table I).

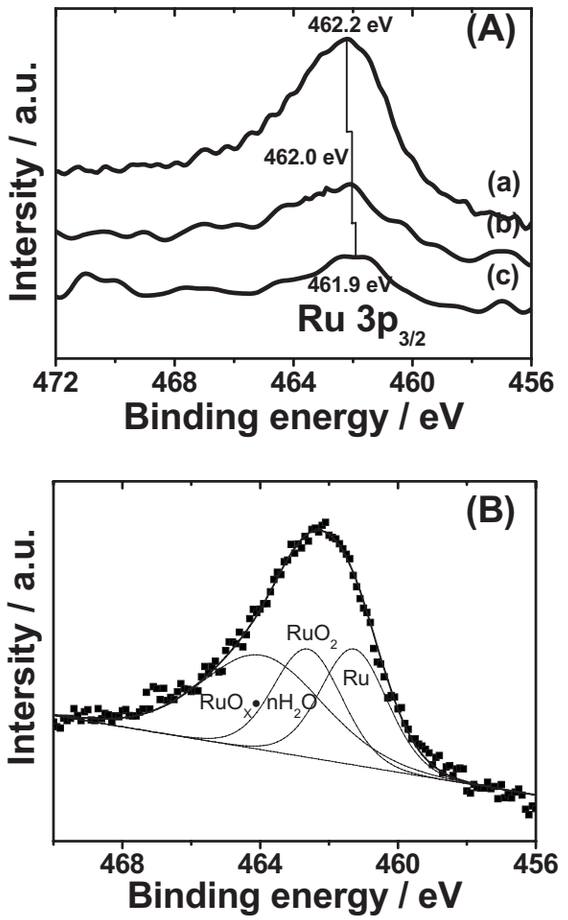

Figure 8. (A) XPS signals of Ru ($3p_{3/2}$) from PtRu nanoparticles with fixed values of T_{on} (50 ms), J_a (50 mA/cm^2), and coulombic charge (8.0 C/cm^2), as well as T_{off} in (a) 100, (b) 400, and (c) 600 ms. (B) The results of curve fitting using Ru^0, RuO_2, and $RuO_2{\cdot}nH_2O$.

cating that the amount of Ru, regardless of its oxidative states, decreases when the duty is reduced. This is consistent with our argument of steady Ru loss during T_{off}.

In an acidic environment, we suspect the possible oxidation states of Ru are Ru^0, RuO_2, and $RuO_2{\cdot}nH_2O$. To determine their relative ratios quantitatively, we carried out curve fitting using software (Thermo Avantage 3.20). The corresponding peaks for RuO_2, and $RuO_2{\cdot}nH_2O$ were 462.2 and 463.8 eV, respectively.[45,48] Shown in Fig. 8b, we acquired a reasonable match for the observed XPS responses. The detailed fitting results are listed in Table VIII. When the T_{off} was prolonged, we observed that the ratio for the metallic Ru increased, while the ratio for the $RuO_2{\cdot}nH_2O$ decreased steadily. Interestingly, the ratio for the RuO_2 remained unchanged. Because the metallic Ru existed in the alloyed state buried inside the PtRu nanoparticles, the loss of Ru in the displacement reaction was likely from the $RuO_2{\cdot}nH_2O$ on the surface.

Table VIII. Results from XPS and curve fitting of PtRu nanoparticles with fixed values of T_{on} (50 ms), J_a (50 mA/cm^2), and total coulombic charge (8.0 C/cm^2).

T_{off} (ms)	Binding energy[a] (eV)	Reference binding energy[b] (eV)	Suggested species	Ratio (%)
100	461.1	461.1	Ru	36.5
	462.6	462.2	RuO_2	33.9
	463.9	463.8	$RuO_2{\cdot}nH_2O$	29.6
400	461.1	461.1	Ru	41.1
	462.4	462.2	RuO_2	34.5
	463.8	463.8	$RuO_2{\cdot}nH_2O$	24.4
600	461.2	461.1	Ru	43.8
	462.4	462.2	RuO_2	36.4
	463.8	463.8	$RuO_2 \cdot nH_2O$	19.8

[a] From XPS curve fitting.
[b] From Ref. 45, 46, and 48.

Conclusion

The pc depositions were employed to prepare PtRu nanoparticles on carbon clothes. Parameters including T_{on}, T_{off}, and J_a were explored to identify the optimized catalytic performances for methanol electro-oxidation. TEM images on the PtRu nanoparticles revealed an uniform distribution with moderate size variations. Measurements from ICP-MS indicated that a displacement reaction was occurring, resulting in the enrichment of Pt in the PtRu nanoparticles when the duty cycle was shortened. XRD analysis on the PtRu nanoparticles exhibited a slight shift of diffraction peaks, suggesting the Ru was alloyed with Pt successfully. In addition, the alloyed Ru was found to decrease with reduced duty cycles. Analysis from XPS confirmed a steady loss of $RuO_2{\cdot}nH_2O$ when the T_{off} was prolonged.

Acknowledgments

Financial support from the National Science Council of Taiwan is noted (NSC-96-2221-E-009-110).

National Chiao Tung University assisted in meeting the publication costs of this article.

References

1. B. C. H. Steele and A. Heinzel, *Nature (London)*, **414**, 345 (2001).
2. G. J. K. Acres, *J. Power Sources*, **100**, 60 (2001).
3. H. Liu, C. Song, L. Zhang, J. Zhang, H. Wang, and D. P. Wilkinson, *J. Power Sources*, **155**, 95 (2006).
4. O. A. Petrii, *J. Solid State Electrochem.*, **12**, 609 (2008).
5. H. Igarashi, T. Fujino, Y. Zhu, H. Uchida, and M. Watanabe, *Phys. Chem. Chem. Phys.*, **3**, 306 (2001).
6. P. Strasser, Q. Fan, M. Devenney, W. H. Weinberg, P. Liu, and J. K. Nørskov, *J. Phys. Chem. B*, **107**, 11013 (2003).
7. J. F. Whitacre, T. Valdez, and S. R. Narayanan, *J. Electrochem. Soc.*, **152**, A1780 (2005).
8. T. Yajima, H. Uchida, and M. Watanabe, *J. Phys. Chem. B*, **108**, 2654 (2004).
9. P. Waszczuk, G. Q. Lu, A. Wieckowski, C. Lu, C. Rice, and R. I. Masel, *Electrochim. Acta*, **47**, 3637 (2002).
10. F. Richarz, B. Wohlmann, U. Vogel, H. Hoffschulz, and K. Wandelt, *Surf. Sci.*, **335**, 361 (1995).
11. J. H. Choi, K. W. Park, B. K. Kwon, and Y. E. Sung, *J. Electrochem. Soc.*, **150**, A973 (2003).
12. S. Y. Huang, S. M. Chang, and C. T. Yeh, *J. Phys. Chem. B*, **110**, 234 (2006).
13. M. C. Tsai, T. K. Yeh, and C. H. Tsai, *Electrochem. Commun.*, **8**, 1445 (2006).
14. J. M. Sieben, M. M. E. Duarte, and C. E. Mayer, *J. Appl. Electrochem.*, **38**, 483 (2008).
15. C. Coutanceau, A. F. Rakotondrainibé, A. Lima, E. Garnier, S. Pronier, J. M. Léger, and C. Lamy, *J. Appl. Electrochem.*, **34**, 61 (2004).
16. F. Alcaide, Ó. Miguel, and H. J. Grande, *Catal. Today*, **116**, 408 (2006).
17. Z. D. Wei and S. H. Chan, *J. Electroanal. Chem.*, **569**, 23 (2004).
18. A. Bauer, E. L. Gyenge, and C. W. Oloman, *J. Power Sources*, **167**, 281 (2007).
19. S. S. Kim, Y. C. Nah, Y. Y. Noh, J. Jo, and D. Y. Kim, *Electrochim. Acta*, **51**, 3814 (2006).
20. Z. D. Wei, S. G. Chen, Y. Liu, C. X. Sun, Z. G. Shao, and P. K. Shen, *J. Phys. Chem. C*, **111**, 15456 (2007).
21. J. Lee, J. Seo, K. Han, and H. Kim, *J. Power Sources*, **163**, 349 (2006).
22. K. H. Choi, H. S. Kim, and T. H. Lee, *J. Power Sources*, **75**, 230 (1998).
23. S. Roy, M. Matlosz, and D. Landolt, *J. Electrochem. Soc.*, **141**, 1509 (1994).
24. S. Roy and D. Landolt, *J. Electrochem. Soc.*, **142**, 3021 (1995).
25. Q. Zhu and C. L. Hussey, *J. Electrochem. Soc.*, **148**, C395 (2001).
26. L. Magagnin, R. Maboudian, and C. Carraro, *J. Phys. Chem. B*, **106**, 401 (2002).
27. J. Zhang, F. H. B. Lima, M. H. Shao, K. Sasaki, J. X. Wang, J. Hanson, and R. R. Adzic, *J. Phys. Chem. B*, **109**, 22701 (2005).
28. M. B. Vukmirovic, J. Zhang, K. Sasaki, A. U. Nilekar, F. Uribe, M. Mavrikakis, and R. R. Adzic, *Electrochim. Acta*, **52**, 2257 (2007).
29. C. Thambidurai, Y. G. Kim, and J. L. Stickney, *Electrochim. Acta*, **53**, 6157 (2008).

30. L. A. Porter, Jr., H. C. Choi, A. E. Ribbe, and J. M. Buriak, *Nano Lett.*, **2**, 1067 (2002).
31. S. R. Brankovic, J. McBreen, and R. R. Adžić, *J. Electroanal. Chem.*, **503**, 99 (2001).
32. S. R. Brankovic, J. X. Wang, and R. R. Adžić, *Electrochem. Solid-State Lett.*, **4**, A217 (2001).
33. S. R. Brankovic, J. X. Wang, Y. Zhu, R. Sabatini, J. McBreen, and R. R. Adžić, *J. Electroanal. Chem.*, **524–525**, 231 (2002).
34. R. J. Woods, *Electroanal. Chem.*, **9**, 1 (1976).
35. Z. Liu, X. Y. Ling, B. Guo, L. Hong, and J. Y. Lee, *J. Power Sources*, **167**, 272 (2007).
36. T. Frelink, W. Visscher, and J. A. R. van Veen, *Surf. Sci.*, **335**, 353 (1995).
37. C. L. Green and A. Kucernak, *J. Phys. Chem. B*, **106**, 11446 (2002).
38. F. Maillard, F. Gloaguen, and J.-M. Leger, *J. Appl. Electrochem.*, **33**, 1 (2003).
39. F. Vigier, F. Gloaguen, J.-M. Leger, and C. Lamy, *Electrochim. Acta*, **46**, 4331 (2001).
40. A. N. Gavrilov, O. A. Petrii, A. A. Mukovnin, N. V. Smirnova, T. V. Levchenko, and G. A. Tsirlina, *Electrochim. Acta*, **52**, 2775 (2007).
41. T. D. Avtokratova, *Analytical Chemistry of Ruthenium*, p. 8, Ann Arbor-Humphery Science Publishers, Ann Arbor, MI (1963).
42. A. J. Blake, R. O. Gould, B. F. G. Johnson, and E. Parisini, *Acta Crystallogr., Sect. C: Cryst. Struct. Commun.*, **48**, 982 (1992).
43. J. A. Bennett, Y. Show, S. Wang, and G. M. Swain, *J. Electrochem. Soc.*, **152**, E184 (2005).
44. E. Antolini and F. Cardellini, *J. Alloys Compd.*, **315**, 118 (2001).
45. J. S. Spendelow and A. Wieckowski, *Phys. Chem. Chem. Phys.*, **6**, 5094 (2004).
46. XPS Database, U.S. National Institute of Standards and Technology, Gaithersburg, MD (2008).
47. A. Lewera, W. P. Zhou, R. Hunger, W. Jaegermann, A. Wieckowski, S. Yockel, and P. S. Bagus, *Chem. Phys. Lett.*, **447**, 39 (2007).
48. K. H. Chang and C. C. Hu, *J. Electrochem. Soc.*, **151**, A958 (2004).